A stable Runge-Kutta discontinuous Galerkin solver for hypersonic rarefied gaseous flows

Wei Su, Bijiao He, and Guobiao Cai

Citation: AIP Conference Proceedings **1628**, 980 (2014); doi: 10.1063/1.4902700
View online: http://dx.doi.org/10.1063/1.4902700
View Table of Contents: http://scitation.aip.org/content/aip/proceeding/aipcp/1628?ver=pdfcov
Published by the AIP Publishing

A Stable Runge-Kutta Discontinuous Galerkin Solver for Hypersonic Rarefied Gaseous Flows

Wei Su, Bijiao He and Guobiao Cai

School of Astronautics, Beihang University, Beijing 100191, China

Abstract. A stable high-order discontinuous Galerkin scheme which strictly preserves the positivity of the solution is designed to solve the Boltzmann kinetic model equations. The stability is kept by the accuracy of the velocity discretization, the conservation of the collision terms and a limiter. By requiring the time step smaller than the local mean collision time and forcing positive values of velocity distributions on certain points, the limiter can preserve the positivity of the solutions of the cell average velocity distributions. Verification is performed with a normal shock wave at Mach number of 2.05 and a supersonic flow about a 2D cylinder at Mach number of 6.0.

Keywords: high-order discontinous Galerkin, positivity-preserving limiter, model equations, hypersonic flows
PACS: 02.60.Cb, 47.11.Fg, 47.45.-n

INTRODUCTION

Direct solvers of Boltzmann kinetic models have been widely developed due to their efficiency in resolving near continuum flows, micro-scale flows and unsteady flows. In these approaches, the control equations are firstly discretized in velocity space and cast into a system of partial differential equations which depend on physical coordinates and time. Then the discrete equations are solved using CFD methods. The Runge-Kutta discontinuous Galerkin (RKDG) method is a finite element formalism which is well suited for solutions of time-dependent hyperbolic equations. Compared with other high-order methods such as finite difference method (FDM) and finite volume method (FVM), it is more efficient in discretization with the same order of accuracy [1]. Other advantages of the RKDG method include easy formulation on irregular meshes, straightforward implementation of boundary conditions, as well as efficient parallel computation. In our previous work, we have developed a conservative RKDG scheme for 2D/2V and 2D/3V Boltzmann kinetic equations with the Bhatnagar-Gross-Krook (BGK) and the ellipsoidal statistical BGK (ES-BGK) models. It offers a conservative formulation of the collision relaxation term within high-order method on arbitrary triangular meshes [2].

The RKDG method resolves solutions in piecewise finite element space combining with an explicit-multistep Runge-Kutta time marching. Borrowing from FVM and FDM, the numerical fluxes are evaluated at edges of the physical elements. The approach is stable under a certain CFL conditions when the solutions are smooth or have weak discontinuities [3]. However, when strong discontinuities appear in the field, the approximate solutions exhibit spurious oscillations, which make the iteration unstable. Several limiters have been designed to deal with the non-physical oscillations, such as the TVB limiters [4], moment-based limiters [5], WENO limiters [6, 7] and recently the bound-preserving limiters [8, 9].

In this work, we develop a stable RKDG solver for kinetic models to simulate the hypersonic rarefied gaseous flows. Three essences determine the stability: the accuracy of the velocity discretization, the conservation of the collision terms and a limiter. Based on the maximum-principle-satisfying scheme for scalar conservation laws [9], a positivity limiter is designed for the Boltzmann kinetic models with source terms. The normal shock and hypersonic flow about a 2D cylinder are used to validate the proposed solver.

KINETIC MODELS AND BASIC RKDG METHOD

The kinetic models solved here are the BGK and ES-BGK models written as

$$\partial_t f + \boldsymbol{c} \cdot \nabla_{\boldsymbol{r}} f = \nu(f_{\mathrm{E}} - f), \tag{1}$$

Proceedings of the 29th International Symposium on Rarefied Gas Dynamics
AIP Conf. Proc. 1628, 980-987 (2014); doi: 10.1063/1.4902700

where, f is the molecular velocity distribution function, while $\boldsymbol{c}$ and $\boldsymbol{r}$ are the velocity and spatial coordinates. ν is the collision frequency and f_{E} is a proper equilibrium distribution. In BGK model f_{E} is the local Maxwell distribution, and the one in ES-BGK model is a local anisotropic Gaussian.

A widely used approach to solve the kinetic model equations is the so-called discrete ordinate method. It uses a numerical quadrature to approximate the exact integration over velocity space on a set of discrete velocities. Both the Cartesian and spherical meshes have been developed for velocity discretization [2]. The Cartesian mesh adopts the composite Newton-Cotes formulas and has finite limits which must be chosen carefully to ensure that the effects of the tails of the distribution function are negligible, while the spherical one involves Gaussian-Laguerre quadrature and has no bound limitation. The accuracy of the velocity discretization highly depends on the localization of the distributions. For hypersonic flows, the appropriate velocity ranges could become quite wide and a large number of discrete velocities are needed to meet the accuracy requirement. Therefore, the composite Newton-Cotes formulas are more convenient. In this work, the first-order mid-point rule and the second-order Simpson's rule are used. By introducing N nodes $\boldsymbol{c}^j$ with equal space, eq. (1) is cast into a system of partial differential equations

$$\partial_t f^j + \boldsymbol{c}^j \cdot \nabla_{\boldsymbol{r}} f^j = \nu(f_{\mathrm{E}}^j - f^j) \tag{2}$$

with $f^j = f(t, \boldsymbol{c}^j, \boldsymbol{r})$.

Then the RKDG method is used to solve the control system. The 2D computational domain is partitioned with triangulations $\{\Delta_i\}_{i=1}^M$ and the approximate solutions are sought in the finite element space of piecewise polynomials. The basis adopted here is a local orthogonal one [7] so that the first degree of freedom is the average value on the local triangular cell Δ_i. In order to determine the approximate solution, the standard techniques of the finite element method are applied to obtain the weak formulations, which are expressed as

$$\frac{\mathrm{d}}{\mathrm{d}t} F_l^j = \frac{1}{w^l} \left[\boldsymbol{c}^j \cdot \int_{\Delta_i} f^j \nabla_{\boldsymbol{r}} \varphi_l \,\mathrm{d}x\mathrm{d}y - \int_e h_e^j \varphi_l \,\mathrm{d}\Gamma + \int_{\Delta_i} \nu \left(f_{\mathrm{E}}^j - f^j \right) \varphi_l \,\mathrm{d}x\mathrm{d}y \right], \tag{3}$$

where, F_l^j is the degrees of freedom, φ_l is the basis functions, w^l is the diagonal components of the mass matrix and h_e^j is the numerical fluxes. Since the values of f^j at the edges of the triangles calculated from the adjacent cells are not required equal, the fluxes borrowed from FVM and FDM are calculated based on Riemann solvers. We employ the most simple upwind scheme and write it as

$$h_e^j = h_e(f_{e,\mathrm{int}}^j, f_{e,\mathrm{ext}}^j, \boldsymbol{n}_e) = \frac{1}{2} \left[\boldsymbol{c}^j \cdot \boldsymbol{n}_e f_{e,\mathrm{int}}^j + \boldsymbol{c}^j \cdot \boldsymbol{n}_e f_{e,\mathrm{ext}}^j - |\boldsymbol{c}^j \cdot \boldsymbol{n}_e| \left(f_{e,\mathrm{ext}}^j - f_{e,\mathrm{int}}^j \right) \right], \tag{4}$$

where $\boldsymbol{n}_e$ is the outward unit normal to the edge, $f_{e,\mathrm{int}}^j$ is the approximate solution obtained from the interior of the triangle Δ_i, and $f_{e,\mathrm{ext}}^j$ the one obtained from the exterior of Δ_i. It is easy to show that the upwind flux satisfies the conservativity and consistency

$$h_e^j(f_{e,\mathrm{int}}^j, f_{e,\mathrm{ext}}^j, \boldsymbol{n}_e) = -h_e^j(f_{e,\mathrm{ext}}^j, f_{e,\mathrm{int}}^j, -\boldsymbol{n}_e), \quad h_e^j(f_e^j, f_e^j, \boldsymbol{n}_e) = \boldsymbol{c}^j \cdot \boldsymbol{n}_e f_e^j. \tag{5}$$

Moreover, five different types of boundary conditions are incorporated to specify the boundary values of f_{ext} [2].

Finally, the resulting system of ordinary differential equations is discretized in time by a special class of explicit total variation diminishing (TVD) Runge-Kutta schemes [10]. At each intermediate time step, the equilibrium distribution f_{E} is represented by consistently high-order polynomials. The corresponding degrees of freedom of f_{E} are evaluated such that the conservation of mass, momentum and energy are enforced. In this way, the same high-order discretization of all terms of the Boltzmann kinetic equations is obtained, and the conservative nature with respect to the collision term is preserved. The latter property is very essential to iterations convergence, especially for the low Kn number flows [11].

POSITIVITY-PRESERVING LIMITER FOR HYPERSONIC FLOWS

The RKDG scheme is a shock-capture scheme, which may automatically capture the discontinuities in solutions even if the initial conditions are smooth. It has been proven that this method is energy stable so that it could directly

TABLE 1. The quadrature points and weights for the triangles.

	ξ_1	ξ_2	ξ_3	$W/\lvert\Delta_i\rvert$
edge points	0	$\frac{1}{2}+v_\beta$	$\frac{1}{2}-v_\beta$	$\frac{2}{3}w_1\omega_\beta$
	$\frac{1}{2}+v_\beta$	0	$\frac{1}{2}-v_\beta$	$\frac{2}{3}w_1\omega_\beta$
	$\frac{1}{2}+v_\beta$	$\frac{1}{2}-v_\beta$	0	$\frac{2}{3}w_1\omega_\beta$
interior points	$\frac{1}{2}+v_\beta$	$\left(\frac{1}{2}+u_2\right)\left(\frac{1}{2}-v_\beta\right)$	$\left(\frac{1}{2}-u_2\right)\left(\frac{1}{2}-v_\beta\right)$	$\frac{2}{3}\left(\frac{1}{2}-v_\beta\right)w_2\omega_\beta$
	$\left(\frac{1}{2}-u_2\right)\left(\frac{1}{2}-v_\beta\right)$	$\frac{1}{2}+v_\beta$	$\left(\frac{1}{2}+u_2\right)\left(\frac{1}{2}-v_\beta\right)$	$\frac{2}{3}\left(\frac{1}{2}-v_\beta\right)w_2\omega_\beta$
	$\left(\frac{1}{2}+u_2\right)\left(\frac{1}{2}-v_\beta\right)$	$\left(\frac{1}{2}-u_2\right)\left(\frac{1}{2}-v_\beta\right)$	$\frac{1}{2}+v_\beta$	$\frac{2}{3}\left(\frac{1}{2}-v_\beta\right)w_2\omega_\beta$

be used to solve control equations with smooth solutions or solutions with weak discontinuities [12]. However, for solutions with strong shocks, RKDG scheme will generate spurious oscillations near discontinuities. Because of the oscillations, the numerical solutions of the velocity distribution functions may become negative, which is either non-physical or could lead to instability and non-convergence of iterations. Usually, some forms of limiters are utilized to keep the scheme stable. Treated as post-processor of the approximate solutions, a limiter uses a new polynomial to replace the old one which is deemed to contain oscillations or non-physical values. In order to obtain reasonable results, the new polynomials are required to keep the accuracy and conservativity of the solutions. In [8, 9], limiters have been developed to preserve the maximum principle for DG or FVM schemes solving two-dimensional scalar conservation law on triangular meshes and to preserve positivity for DG schemes solving one-dimensional compressible Euler equations involving the source term. Using the same methodology, we design a positivity-preserving limiter to solve the Boltzmann kinetic model equations on arbitrary triangular meshes, independent of the discrete collision operator.

The Boltzmann kinetic model equations are scalar conservative laws with source terms. First of all, applying the first-order Euler forward time discretization to the first weak formulations (Eq. (3)), i,e, the control equations for cell averages $\bar{f}_{\Delta_i}$, we obtain

$$\bar{f}^{n+1}_{\Delta_i} = \bar{f}^{n}_{\Delta_i} - \frac{\Delta t}{|\Delta_i|}\sum_{e=1}^{3}\int_e h_e(f^n_{e,\mathrm{int}}, f^n_{e,\mathrm{ext}}, \boldsymbol{n}_e)\mathrm{d}\Gamma + \Delta t\overline{\nu(f_{\mathrm{E}}-f)}^n_{\Delta_i}, \tag{6}$$

here, the index n indicates the time steps and the discrete velocity index j has been omitted. For kth-order DG schemes, the edge integral $\int_e \cdot\mathrm{d}\Gamma$ should be approximated by the $(k+1)$-point Gaussian rule. Then, Eq. (6) becomes

$$\bar{f}^{n+1}_{\Delta_i} = \bar{f}^{n}_{\Delta_i} - \frac{\Delta t}{|\Delta_i|}\sum_{e=1}^{3}\sum_{\beta=1}^{k+1}\omega_\beta h_e(f^{n,\beta}_{e,\mathrm{int}}, f^{n,\beta}_{e,\mathrm{ext}}, \boldsymbol{n}_e)s_e + \Delta t\overline{\nu(f_{\mathrm{E}}-f)}^n_{\Delta_i}, \tag{7}$$

where, ω_β is the quadrature weights of the Gauss rule on interval $[-\frac{1}{2},\frac{1}{2}]$ with $\sum_{\beta=1}^{k+1}\omega_\beta = 1$ and s_e is the length of the edge e. In order to rewrite the right hand side of Eq. (7) as a monotone increasing function of some point values of f^n under a certain CFL condition, a special rule is introduced to discretize the triangular integral [9]. The rule combines with 3-point Guass-Lobatto rule and $(k+1)$-point Gaussian rule, which is exact for a polynomial $f(x,y)$ if its degree is not larger than k. Giving the points and weights of Guass-Lobatto rule on interval $[-\frac{1}{2},\frac{1}{2}]$ as $\{u_\alpha, w_\alpha, \alpha = 1,...,3\}$ and the ones of Gaussian rule as $\{v_\beta,\omega_\beta,\beta = 1,...,k+1\}$, the triangle quadrature points indicated by area coordinates $\boldsymbol{x}_\delta(x,y) = (\xi_1,\xi_2,\xi_3)_\delta$ and their relative weights W_δ are listed in Table 1. The quadrature points contain $3(k+1)$ points on the triangle edges which are coincident with the ones of Gaussian quadrature rule, another $3(k+1)$ points on the interior of the triangle. Then the cell average values $\bar{Q}^n_{\Delta_i}$ is expressed as

$$\bar{Q}^n_{\Delta_i} = \sum_{e=1}^{3}\sum_{\beta=1}^{k+1}\frac{2}{3}w_1\omega_\beta Q^{n,\beta}_{e,\mathrm{int}} + \sum_{\gamma=1}^{3(k+1)} Q^n_{\mathrm{int},\gamma}\tilde{w}_\gamma, \tag{8}$$

where $Q^n_{\mathrm{int},\gamma}$ is the point values of the interior and $\tilde{w}_\gamma$ is their weights.

Using the conservativity of the flux, the flux integral is decomposed as

$$\begin{aligned}\sum_{e=1}^{3} h_e(f_{e,\mathrm{int}}^{n,\beta}, f_{e,\mathrm{ext}}^{n,\beta}, \boldsymbol{n}_e)s_e &= h(f_{1,\mathrm{int}}^{n,\beta}, f_{1,\mathrm{ext}}^{n,\beta}, \boldsymbol{n}_1)s_1 + h(f_{2,\mathrm{int}}^{n,\beta}, f_{2,\mathrm{ext}}^{n,\beta}, \boldsymbol{n}_2)s_2 + h(f_{3,\mathrm{int}}^{n,\beta}, f_{3,\mathrm{ext}}^{n,\beta}, \boldsymbol{n}_3)s_3 \\ &= h(f_{1,\mathrm{int}}^{n,\beta}, f_{1,\mathrm{ext}}^{n,\beta}, \boldsymbol{n}_1)s_1 + h(f_{1,\mathrm{int}}^{n,\beta}, f_{2,\mathrm{int}}^{n,\beta}, -\boldsymbol{n}_1)s_1 \\ &+ h(f_{2,\mathrm{int}}^{n,\beta}, f_{1,\mathrm{int}}^{n,\beta}, \boldsymbol{n}_1)s_1 + h(f_{2,\mathrm{int}}^{n,\beta}, f_{2,\mathrm{ext}}^{n,\beta}, \boldsymbol{n}_2)s_2 + h(f_{2,\mathrm{int}}^{n,\beta}, f_{3,\mathrm{int}}^{n,\beta}, \boldsymbol{n}_3)s_3 \\ &+ h(f_{3,\mathrm{int}}^{n,\beta}, f_{2,\mathrm{int}}^{n,\beta}, -\boldsymbol{n}_3)s_3 + h(f_{3,\mathrm{int}}^{n,\beta}, f_{3,\mathrm{ext}}^{n,\beta}, \boldsymbol{n}_3)s_3.\end{aligned} \tag{9}$$

Then, substituting Eqs. (8) and (9) into Eq. (7), we have

$$\begin{aligned}\overline{f}_{\Delta_i}^{n+1} &= \sum_{\beta=1}^{k+1} \frac{2}{3} w_1 \omega_\beta \left[H_{1,\beta} + H_{2,\beta} + H_{3,\beta} \right] + \sum_{\gamma=1}^{3(k+1)} \tilde{w}_\gamma (1 - \Delta t \nu_{\mathrm{int},\gamma}) f_{\mathrm{int},\gamma}^{n} \\ &+ \Delta t \sum_{e=1}^{3} \sum_{\beta=1}^{k+1} \frac{2}{3} w_1 \omega_\beta \nu_{e,\beta} f_{e,\beta}^{E} + \Delta t \sum_{\gamma=1}^{3(k+1)} \tilde{w}_\gamma \nu_{\mathrm{int},\gamma} f_{\mathrm{int},\gamma}^{E},\end{aligned} \tag{10}$$

where, $\nu_{e,\beta}$, $\nu_{\mathrm{int},\gamma}$, $f_{e,\beta}^{E}$ and $f_{\mathrm{int},\gamma}^{E}$ are the point values of collision frequency and equilibrium distribution, and they are all positive values due to the ways, through which they are calculated. The functions $H_{e,\beta}$ are

$$\begin{aligned}H_{1,\beta} &= (1 - \Delta t \nu_{1,\beta}) f_{1,\mathrm{int}}^{n,\beta} - \frac{3\Delta t}{2 w_1 |\Delta_i|} \left[h(f_{1,\mathrm{int}}^{n,\beta}, f_{1,\mathrm{ext}}^{n,\beta}, \boldsymbol{n}_1)s_1 + h(f_{1,\mathrm{int}}^{n,\beta}, f_{2,\mathrm{int}}^{n,\beta}, -\boldsymbol{n}_1)s_1 \right], \\ H_{2,\beta} &= (1 - \Delta t \nu_{2,\beta}) f_{2,\mathrm{int}}^{n,\beta} - \frac{3\Delta t}{2 w_1 |\Delta_i|} \left[h(f_{2,\mathrm{int}}^{n,\beta}, f_{1,\mathrm{int}}^{n,\beta}, \boldsymbol{n}_1)s_1 + h(f_{2,\mathrm{int}}^{n,\beta}, f_{2,\mathrm{ext}}^{n,\beta}, \boldsymbol{n}_2)s_2 + h(f_{2,\mathrm{int}}^{n,\beta}, f_{3,\mathrm{int}}^{n,\beta}, \boldsymbol{n}_3)s_3 \right], \\ H_{3,\beta} &= (1 - \Delta t \nu_{3,\beta}) f_{3,\mathrm{int}}^{n,\beta} - \frac{3\Delta t}{2 w_1 |\Delta_i|} \left[h(f_{3,\mathrm{int}}^{n,\beta}, f_{2,\mathrm{int}}^{n,\beta}, -\boldsymbol{n}_3)s_3 + h(f_{3,\mathrm{int}}^{n,\beta}, f_{3,\mathrm{ext}}^{n,\beta}, \boldsymbol{n}_3)s_3 \right].\end{aligned} \tag{11}$$

Taking $H_{2,\beta}$ as an example to discuss its property, the function is rewritten as

$$H_{2,\beta} = \left(1 - \Delta t \nu_{2,\beta} - \frac{3\Delta t}{2 w_1 |\Delta_i|} \cdot \frac{\sum_{e=1}^{3} |\boldsymbol{c} \cdot \boldsymbol{n}_e| s_e}{2} \right) f_{2,\mathrm{int}}^{n,\beta} - \frac{3\Delta t}{4 w_1 |\Delta_i|} \sum_{e=1}^{3} s_e (\boldsymbol{c} \cdot \boldsymbol{n}_e - |\boldsymbol{c} \cdot \boldsymbol{n}_e|) f_{e,\mathrm{int}}^{n,\beta}. \tag{12}$$

Therefore, under the following condition,

$$1 - \Delta t \nu_{2,\beta} - \frac{3\Delta t}{2 w_1 |\Delta_i|} \cdot \frac{\sum_{e=1}^{3} |\boldsymbol{c} \cdot \boldsymbol{n}_e| s_e}{2} \geq 0, \tag{13}$$

the function $H_{2,\beta}$ is a monotone increasing function of $f_{2,\mathrm{int}}^{n,\beta}$, $f_{1,\mathrm{int}}^{n,\beta}$, $f_{2,\mathrm{ext}}^{n,\beta}$ and $f_{3,\mathrm{int}}^{n,\beta}$. Similarly, under the conditions

$$1 - \Delta t \nu_{1,\beta} - \frac{3\Delta t}{2 w_1 |\Delta_i|} \cdot |\boldsymbol{c} \cdot \boldsymbol{n}_1| s_1 \geq 0, \quad 1 - \Delta t \nu_{3,\beta} - \frac{3\Delta t}{2 w_1 |\Delta_i|} \cdot |\boldsymbol{c} \cdot \boldsymbol{n}_3| s_3 \geq 0, \tag{14}$$

the functions $H_{1,\beta}$ and $H_{3,\beta}$ are also monotone increasing functions of the point values.

Finally, writing the right-hand side of Eq. (10) as a function of all the point values of f^n, this function is monotone increasing with respect to each argument under Eq. (13) and Eq. (14) plus $(1 - \Delta t \nu_{\mathrm{int},\gamma}) \geq 0$. Therefore, if all the point values $f^n(\boldsymbol{x}_\delta)$ at time step t^n are non-negative, the average value $\tilde{f}_{\Delta_i}^{n+1}$ will still be positive at the next time step t^{n+1}. Similar result holds for other monotone fluxes [9].

Then we obtain the sufficient conditions to preserve the positivity of the distribution functions. Firstly, the time interval should satisfy the CFL condition

$$\Delta t \leq \frac{1}{A + \nu_{\max}}, \quad A = \frac{3}{2 w_1 |\Delta_i|} \max \left\{ \frac{1}{2} \sum_{e=1}^{3} |\boldsymbol{c}^j \cdot \boldsymbol{n}_e| s_e, |\boldsymbol{c} \cdot \boldsymbol{n}_e| s_e \right\}, \tag{15}$$

TABLE 2. Conditions across a Normal shock wave of Mach number $Ma = 2.05$.

Property	Upstream	Downstream
Density	1.0	2.334
Temperature	1.0	2.144
Velocity	1.871	0.802

where, $w_1 = \frac{1}{6}$, $\nu_{\max}$ is the maximum collision frequency. Therefore, the time interval must be smaller than the minimum mean collision time. Secondly, the values of the distribution functions on the quadrature points $\boldsymbol{x}_\delta$ should be positive, which is achieved by a linear scaling limiter [9]. At each time step, new polynomials $f^{\text{new}}_{\Delta_i}(x,y)$ is constructed to replace the solutions $f^n_{\Delta_i}(x,y)$ which is defined as

$$f^{\text{new}}_{\Delta_i}(x,y) = \theta\left(f^n_{\Delta_i}(x,y) - \overline{f}^n_{\Delta_i}\right) + \overline{f}^n_{\Delta_i}, \quad \theta = \min\left\{\frac{\overline{f}^n_{\Delta_i} - \epsilon}{\overline{f}^n_{\Delta_i} - f_{\min}}, 1\right\} \tag{16}$$

with

$$f_{\min} = \min_{\delta} f^k_{\Delta_i}(\boldsymbol{x}_\delta), \quad \epsilon = \min_i \left\{10^{-20}, |\overline{f}^n_{\Delta_i}|\right\}. \tag{17}$$

This limiter retains the accuracy and conservativity of the solutions.

Since the high-order Runge-Kutta time discretization is a convex combinations of Euler forward scheme, the full schemes with high-order time discretization will still satisfy the positivity preserving property of the cell average values [9].

RESULTS AND DISCUSSIONS

In this section, we provide numerical results to demonstrate the performance of the positivity limiter for RKDG method on triangular meshes described in the previous section. The density and temperature profiles of the flow fields are obtained using second and third order RKDG schemes. The solutions are compared with those obtained from experimental data and DSMC calculations. The numerical schemes were implemented in C++ and MPI was used for the parallel version of the code.

Normal Shock Wave

We first test the accuracy of the schemes. The results presented below were computed from a normal shock wave in Argon gas at Mach number of $M_1 = 2.05$. At this Mach number condition, the RKDG schemes are stable even without limiters. The same parameters as in the experiments by Alsmeyer [13] were used here with upstream density $\rho_1 = 1.067 \times 10^{-4}$ kg/m^3 and temperature $T_1 = 300$ K, corresponding to the mean free path of the hard sphere models as $\lambda_1 = 1.098 \times 10^{-3}$ m. The non-dimensionalized boundary conditions obtained from the Rankine-Hugoniot relation are shown in TABLE 2. The reference speed is $c_0 = \sqrt{2RT_1}$. The second-order and third-order RKDG methods were used to solve the 2D/3V ES-BGK model on two-dimensional spatial mesh with uniform triangulation. The spatial mesh and boundary conditions are shown in Fig. 1. The length of the domain was $40\lambda_1$. The top and bottom boundaries were symmetries. The left boundary was the hypersonic inlet with upstream condition, and the right boundary was a specular wall moving with the down stream. At the beginning, the $x < 0$ region was initialized with upstream condition while the $x > 0$ region was initialized with the downstream one. The velocity grid of $13 \times 13 \times 13$ discrete velocities with bounds $[-u_2 - 5\sqrt{T_2/2}, u_2 + 5\sqrt{T_2/2}]$ in x direction and $[-5\sqrt{T_2/2}, 5\sqrt{T_2/2}]$ in the other two directions, and the first-order quadrature rule were used. When L_2 norm of the change in velocity distributions with each time-step was less than 10^{-5}, the steady state solutions were assumed to have been reached.

The obtained results are compared with the DSMC solutions, experimental data and analytical results. The DSMC simulation used 300 cells. The average number of molecules per cell was about 50. About 30,000 iterations with a time of 7.5×10^{-8} s were needed to reach steady state. The macro-parameters were sampled over another 50,000

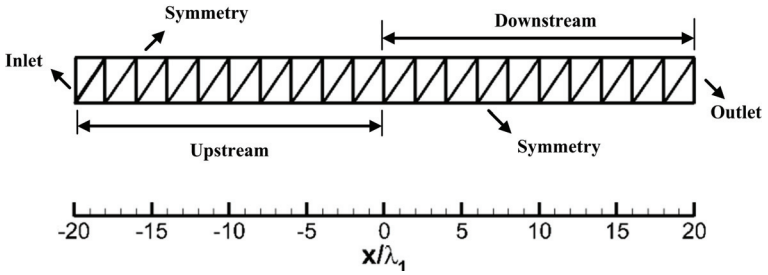

FIGURE 1. Spatial mesh and boundary conditions for normal shock wave.

TABLE 3. Errors of the overshoot temperature. RKDG with the limiter compared to ones without limiter.

Method	Cell number	$\Delta t/\times 10^8$ s	RKDG without limiter			RKDG with limiter		
			iterations	L_1 error	L_∞ error	iterations	L_1 error	L_∞ error
DG-2	16	7.52	3,181	1.67E-2	3.18E-1	3,082	1.56E-2	1.45E-1
	32	3.95	7,328	3.99E-3	1.17E-1	7,247	3.84E-3	9.95E-2
	64	2.03	15,051	1.15E-3	2.10E-2	15,035	1.15E-3	2.10E-2
	128	1.03	30,046	5.46E-4	5.37E-3	30,037	5.46E-4	5.37E-3
DG-3	8	13.70	1,524	1.72E-2	1.53E-1	1,507	2.39E-2	1.26E-1
	16	7.52	3,440	3.25E-3	5.26E-2	3,340	2.68E-3	5.12E-2
	32	3.95	7,475	5.39E-4	2.79E-3	7,448	5.39E-4	2.78E-3
	64	2.03	15,118	4.15E-4	2.04E-3	15,105	4.15E-4	2.04E-3

steps. One of the important properties of a shock wave in a monatomic gas is the overshoot of temperature associated with the longitudinal component of thermal velocities T_x, which is related to the number density n as

$$\frac{T_x}{T_1} = \frac{1}{3}\left[\left(5M_1^2+3\right)\frac{n_1}{n} - 5M_1^2\left(\frac{n_1}{n}\right)^2\right]. \tag{18}$$

Here, we use this parameter as an analytical criterion to demonstrate the errors of the RKDG solutions.

The relative L_1 and L_∞ errors of the overshoot temperature for RKDG method with the positivity-preserving limiter comparing with the original RKDG method without a limiter are shown in TABLE 3. The downstream parameters were used to determine the time step Δt. The DG-2 results of the L_1 and L_∞ errors of the overshoot temperature for 128 triangles reduce to 5.46×10^{-4} and 5.37×10^{-3}, while the DG-3 method obtains the result of the same accuracy on just 32 triangles. For each case with the same computing conditions, the RKDG scheme combining with the positivity-preserving limiter uses a bit fewer iterations to get the steady flow field, and the errors of the solutions are also at the same level. Therefore, the limiter keeps the designed order of accuracy. Figure 2 shows the normalized density $\rho_n = \frac{\rho-\rho_1}{\rho_2-\rho_1}$ and temperature $T_n = \frac{T-T_1}{T_2-T_1}$. The black solid lines are the profiles of DG-3 solution with limiter on 32 triangles, the blue dash dot line is the density distribution from experiment and the red dots illustrate the DSMC results. The proposed scheme captures the normal shock structure very well.

2D Supersonic Flow Past a Cylinder

In this test we consider a flow past a cylinder of radius 0.04m. The free stream gas is Ar with $\rho_\infty = 1.95\times10^{-4}$ kg/m^3, $T_\infty = 200$ K, $M_\infty = 6.0$ for density, temperature and Mach number respectively. The VHS model was used to calculate the viscosity, which gives a Knudsen number Kn of 0.005 at infinity. We choose such a small Kn to test the stability of the schemes, because the flow can generate a strong bow shock passing the cylinder.

The second-order RKDG method was used to solve the 2D/3V BGK model equation on unstructured triangulation with 2,313 triangles. The computational domain was restricted to the upstream flow and the influence of the flow downstream from the cylinder was neglected. We employed the Simpson's quadrature rule and the velocity grid of $35\times35\times35$ points ranging from -11.07 to 11.07 (nondimensionalized by $\sqrt{2RT_\infty}$, where R is the gas constant) in each velocity direction. According to the CFL condition, the time interval of 9.02×10^{-9} s was used, and the time

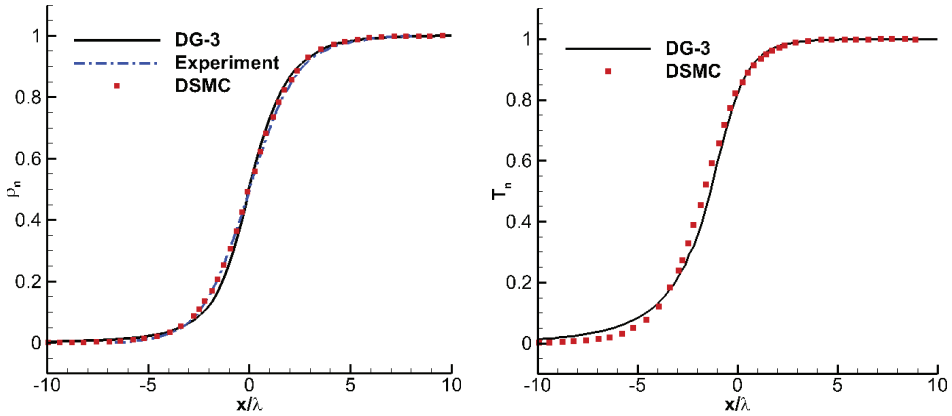

(a) Density profile (b) Temperature profile

FIGURE 2. Normalized density and temperature profiles of normal shock wave.

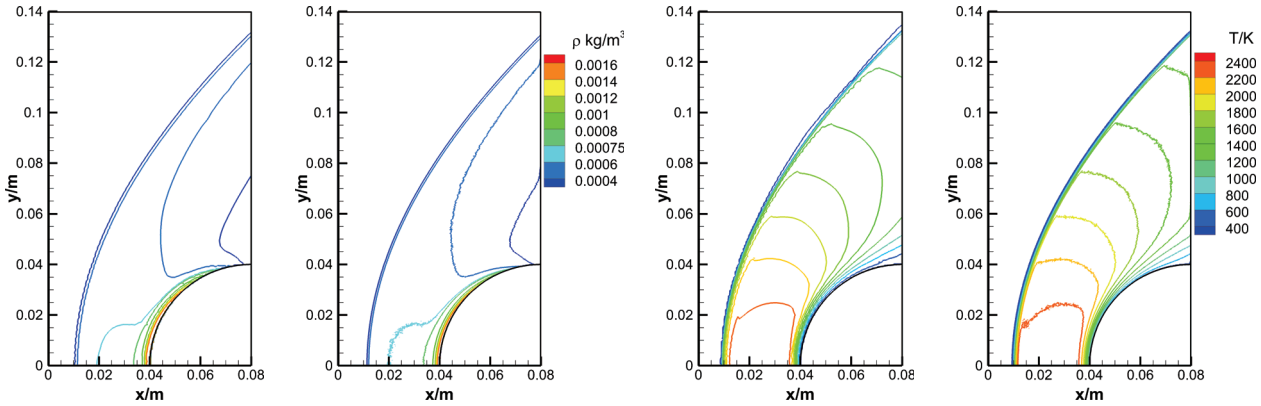

(a) Density DG-2 (b) Density DSMC (c) Temperature DG-2 (d) Temperature DSMC

FIGURE 3. DG-2 and DSMC solutions of hypersonic cylinder flow.

convergence criterion was that the L_2 norm of residual of the velocity distributions decreased by a factor of 10^4. The obtained results are compared with DSMC solutions, which used 400×700 cells and totally 6.18×10^6 molecules. About 30,000 iterations with a time of 1.9×10^{-7} s were needed to reach steady state. The macro-parameters were sampled over another 30,000 steps. The DG-2 solutions of density and temperature contours are shown in Fig. 3 together with the DSMC results. The flow flied structures from both the methods display rather striking similarity.

CONCLUSIONS

A stable RKDG scheme which strictly preserves the positivity of the solutions, has been designed to solve the Boltzmann kinetic model equations for hypersonic rarefied gaseous flows. The stability is kept by the accuracy of the velocity discretization, the conservation of the collision terms and a limiter. For hypersonic flows, the appropriate velocity ranges could become quite wide and a large number of discrete velocities are needed to meet the accuracy requirement. Therefore, the equally-spaced composite Newton-Cotes formulas are more convenient to approximate the velocity integral with appropriate velocity bounds. Based on the first-order Euler forward time discretization and a special triangle quadrature rule, the sufficient conditions which keep the positivity of the cell average solutions of the velocity distributions are obtained. These sufficient conditions require the time step smaller than the minimum local mean collision time, and that the values of velocity distributions on the quadrature points are always non-negative. The later requirement is forced by a linear limiter. Since the high-order Runge-Kutta time discretization is a convex

combination of Euler forward, the full schemes with high-order time discretization will still satisfy the positivity preserving property of the cell average values. Verification of the scheme has been performed by comparison with DSMC and analytical solutions for normal shock wave at Mach number of 2.05 and a hypersonic flow at Mach number of 6.0 passing a 2D cylinder. Results show that, the scheme is stable and accurate to capture the shock structures.

ACKNOWLEDGMENTS

This work is supported by the NSFC grant 11302017 and by National Supercomputer center in Tianjing. All the numerical tests were run on the TH-I cluster. Finally, the authors wish to express their appreciation to Prof. Alina A. Alexeenko for her valuable suggestion and help.

REFERENCES

1. T. Zhou, Y. Li, and C. wang Shu, *Journal of Scientific Computing* **16**, 145–171 (2001).
2. W. Su, A. A. Alexeenko, and G. Cai, "A Runge-Kutta discontinuous Galerkin solver for 2D Boltzmann model equations: Verification and analysis of computational performance," in *AIP Conference Proceedings*, 2012, vol. 1501, pp. 381–388.
3. B. Cockburn, and C.-W. Shu, *Journal of Computational Physics* **141**, 199 – 224 (1998).
4. C.-W. Shu, *Mathematics of Computation* **49**, 105–105 (1987).
5. R. Biswas, K. D. Devine, and J. E. Flaherty, *Applied Numerical Mathematics* **14**, 255–283 (1994).
6. J. Qiu., and C. Shu, *SIAM Journal on Scientific Computing* **26**, 907–929 (2005).
7. J. Zhu, X. Zhong, C.-W. Shu, and J. Qiu, *Journal of Computational Physics* **248**, 200 – 220 (2013).
8. X. Zhang, and C.-W. Shu, *Journal of Computational Physics* **230**, 1238 – 1248 (2011).
9. X. Zhang, Y. Xia, and C.-W. Shu, *Journal of Scientific Computing* **50**, 29–62 (2012).
10. C.-W. Shu, and S. Osher, *Journal of Computational Physics* **77**, 439 – 471 (1988).
11. V. Titarev, and E. Shakhov, *Fluid Dynamics* **40**, 790–804 (2005).
12. G. Jiang, and C.-W. Shu, *Math. Comput.* **62**, 531–538 (1994).
13. H. Alsmeyer, *Journal of Fluid Mechanics* **74**, 497–513 (1976).